

Response to reviewer 1

Dear Anonymous Reviewer 1,

we highly appreciate your feedback. It helped us to improve the manuscript. Below we comment on your suggestions in detail.

GENERAL COMMENT:

The manuscript analyzes data from the Perdigão 2017 campaign to show measurements from sonic anemometers, lidars, and compare those with modeled data.

The use of novel observational techniques, especially in complex terrain, is of great interest for the wind energy community. The technical description of the observations used is well-detailed (maybe even a bit too much), and the plots and figures are generally well-made.

However, the purpose of including modeling data (with a rather poor match with the observations) in this study is not made sufficiently clear in the manuscript, especially when considering the title, abstract, and introduction. As a consequence, the reader can be a bit lost in terms of the main goal and novelty of this piece of literature.

Along these lines, in order to create a more coherent story, the authors shall spend some time adding additional sentences throughout the manuscript describing the meaning and/or causes for the results shown, rather than purely describing the data plotted in the figures or listed in the tables.

Thank you for your comments. We revised the entire manuscript taking into account your comments. Most importantly, we added a Discussion section with the focus on the interpretation of the observed flow structures and the limitation of the WRF-LES simulation. Please find detailed information on our changes below your specific comments and in the attached marked-up version of the manuscript.

SPECIFIC COMMENTS:

1. P.1 l.6: “we found that for different flow conditions on average [...]”is not clear for a reader that has not read the whole paper yet.

See answer for comment 3.

2. P.1 l.7: “depending on the atmospheric conditions” is also too vague.

See answer for comment 3.

3. I think the story you are trying to tell in the abstract is missing some pieces. According to the first part of the abstract, your goal in this study is to demonstrate that scanning lidars can be used to measure wind in complex terrain. And you re-state this at the very end. However, you do not mention

the comparison of the lidar measurements with other instruments to validate your thesis. Then, you mention you simulate the wind flow with WRF-LES to check whether it can represent well the wind flow by comparison with the lidars. And this is not mentioned at all in the title. Please clarify what the actual and final goal (and novelty) of this work is.

Thank you for these detailed comments on the abstract. We reformulated the whole abstract.

4. *P.1 l.17: “cheaper” seems too much of a strong opinion to me. It actually depends.*

„Cheaper“ has been replaced by „can be cost-effective“.

5. *P.2l.5 change to “to assess” or “in assessing”.*

Corrected.

6. *P.2 l.10 “use” instead of “present”.*

Changed.

7. *P.2 l.13: which parallel ridges? Do not assume the reader is familiar with the campaign: you haven’t described it yet.*

The sentence has been reformulated. It now reads: “...of wind resources along two ridges, which favorable sites for wind turbines sides, at the Perdigão site.”.

8. *Introduction: the goal of the study is still not sharp clear. From how this reads, you are plotting data measured by the lidars, and comparing with modeled data. What is the advancement provided by this study? How does this relate with the title of the paper?*

The introduction has been reviewed and describes now clearer the study goals.

9. *P.2 l.20-24: use either all “Section” or “section” throughout.*

Corrected.

10. *Figure 1: can you please center panel c in the figure?*

Done.

11. *Figure 1: please only use either “a.s.l.” or “asl.”*

Corrected.

12. Section 2.1.1: most of this paragraph describes how the 2015 design was chosen. Instead, I would prefer the focus to be on the 2017 design. And refer to the 2015 design simply with something like “By extending the design of the 2015 campaign (reference), ...”.

Thanks for the suggestion. The paragraph has been reformulated accordingly.

13. P.4 l.25: again, I don’t think we need to know how the 2015 were being generated.

This information has been removed.

14. P.4 l.26: “For these reasons, the initial deployment of instruments was complicated and time-consuming.” is probably not needed in a scientific paper.

The content has been removed.

15. Section 2.1: I feel like this whole section has a bit too much details that would be beneficial for a technical report, not so much for the main body of a scientific publication. Please consider moving some details to an appendix/SI. Also, after filtering the relevant information, the division in subsections might not be needed anymore.

Thank you for pointing this out. We restructured and reformulated the section.

16. Table 1: the names of the WindScanners in the table do not match those shown in the maps in Figure 1. Please correct and be consistent.

The naming convention is now consistent throughout the manuscript.

17. P.5 l.19: add “above ground level” after the height of the instruments on the masts.

AGL has been added to the heights of mast-mounted instruments.

18. Section 2.2: you have not mentioned the sonic anemometers anywhere in the abstract or introduction, so now this feels a bit confusing. Please clarify earlier in the text.

The use of sonic measurements for validation purposes of the scanning lidar measurements is now mentioned in the abstract and introduction.

19. P.6 l. 18-20: this is a repetition of what later reported in the data availability section, and as such can be safely removed.

The content has been removed.

20. P.7 l.11: why did you choose 15 range gates and not a different number?

The window size of the moving median such as the thresholds used by the filter have been intensely tuned and tested for the present dataset and has been found to work well in different atmospheric conditions. Different approaches (without success) have been tested to remove fixed thresholds or window sizes from the method.

21. Figure 2: to make the panels larger, you can consider including only one color bar for the whole figure, instead of the four shown now, as they are all the same. Same comment with axis labels. Also, include panel names (a, b, c, d) in the figure.

Thank you, we changed the figure according to the suggestions.

22. Section 4.3: it seems like lidar data are computed as 10-minute average, while the LES data are instantaneous data. If this is the case, please comment on how this difference can impact your comparison between observations and modeled data.

Yes it's correct, that LES data are instantaneous whereas lidar data are 10-minute averages. We think that the usage of 10-minute averaged LES data would improve the comparison with lidar observations. However, in our opinion the forest parameterization including correct tree heights and horizontal distribution of forested areas across the ridges has a larger impact on the comparison of lidar and LES data than different time averaging intervals. This is only our appreciation and should be investigated in further studies.

23. Section 4.2.3: after reading the section, it is still not clear to me which timeframe you are using for your analysis. Only the IOP, or the full period of overlap among all lidars? Please clarify.

The text has been modified to clarify that only periods measured during the IOP period are used. The section reads now as follows: “.... For the analysis, we only use measurement of the IOP period, due to the higher data availability, and removed periods with wind speeds below 3 m s^{-1} at 80 m height (measured at the mast tse04) which leaves 507 10 minute periods, corresponding to 23% of the IOP period.”

24. P.10 l. 13: do you mean “lidar data” here?

As page 10 doesn't have thirteen lines we assume that this comment refers to line 13 on page 9. There the term “sonic data” was used intentionally and correctly. We averaged the sonic data, which is available continuously with a temporal resolution of 20 Hz, for the periods of 500 ms during which the SLs measured closest to the masts. The wording has been improved to make this clearer in the manuscript.

25. Figure 3: what is the temporal period of the comparison shown? Why were only certain wind directions chosen? This should also be specified in the main text, and not only in the figure caption. Also, please make the panels larger.

The information has been added to the caption and the main body of the manuscript: “For this comparison only measurements from IOP are selected, and measurements are limited to the prevailing wind directions ($\pm 15^\circ$ centered around the transect orientated 54° towards north) to minimize the effects of mast wind shadow and to be consistent with the data fraction used for the further analysis.” The figure has been increased in size.

26. Figure 4: the titles of the plots are not consistent with those of Figure 3. Please, larger panels. Why are two regression lines shown in each plot? This is not described in the text.

Figure 3 and figure 4 cannot be compared directly. Figure 3 shows the correlation of radial velocities of the four SLs and the 80 m sonics. Figure 4 shows the correlation of reconstructed wind speeds of the SLs and the horizontal/projected wind speed measured by the sonics at 60 m and 80 m. This is the reason for the different non-consistent titles of the plots. The two regression lines show the correlation of the reconstructed lidar wind speed with the horizontal wind speed and the wind speed projected to the plane spanned by the SLs measured by the sonics anemometers. This has been made clearer in the manuscript.

27. Section 5.1: I think it is important, at the end of the section, to be explicit about the overall purpose of the comparison (which I guess was to validate the lidar data?).

Thanks for this suggestion. A clarifying paragraph of the purpose of the comparison has been added to section 5.1.

28. Figure 5: only one color bar and larger panels, please. Some panels have a “N” label in the top-left corner, some have not: please be consistent.

We updated the figure and it shows now only one color bar as suggested. The label “N” specifies the number of 10-minute periods used per case. The number is identical per case; thus, it is only shown once per case in the plot of the northwest ridge and not repeated in the plot of the southwest ridge.

29. Section 5.2.1 describes the data, but do you have any possible explanation on why what you describe is happening?

We agree that the manuscript missed discussion and explanation of the observed flow structures. We added a whole discussion section (Section 6 of the revised manuscript) to address these points.

30. Table 3: over which time interval is TI (i.e. mean and std) calculated? Same question for TKE. Add “AGL” after “100 m”. Is veer really in degrees? Or degrees per meter?

Thanks for catching these points. They have been corrected in the manuscript.

31. P.13 l.7: where is turbulence dissipation shown in the table?

The term “turbulence dissipation” has been by mistake used for “turbulent kinetic energy”. This has been corrected in the manuscript.

32. P.15: the correlation is quite poor, even for the “best” model setup. This should be pointed out in the text and critically explained.

It is right that the correlations are quite poor. We explain this, however, on page 15 and 16 by means of Wagner et al. 2019b. The forest drag on the ridges is too strong due to too high tree heights and due to a wrong horizontal forest distribution on the ridge tops, which is induced by insufficient landuse data sets. Further model simulations with better forest distribution and more realistic tree heights need to be done in the future to investigate this effect.

33. P.15 l.12: so why you didn’t pick 15m for the modeled tree height?

The tree height of 30 m was chosen when the simulation setup was configurated and no information about actual tree height was available.

34. P. 17 l. 28: rephrase as “In the future, the system availability, which was only at 44% for the period investigated in this study, has to be improved.”

The sentence has been rephrased according to the suggestion.

35. Data availability: “high-resolution”.

Corrected.

36. References: please make sure that all listed references are in the same format. Some titles have capital letters for each word, some have not. Some publications have the DOI not listed.

DOIs have been added to each reference if available. Capitalized titles could not be identified.

Response to reviewer 2

Dear Anonymous Reviewer 2,

we highly appreciate your feedback. It helped us to improve the manuscript. Below we comment on your suggestions in detail.

General comments

The manuscript „Multi-lidar wind resource mapping in complex terrain“ by Robert Menke et al. presents dual Doppler lidar measurements from the Perdigão 2017 campaign and compares them to combined mesoscale and large eddy simulations on the basis of ten minute averages. The presented lidar scan pattern along a line with constant height above a ridge is novel and interesting and could possibly serve in applications for resource assessment in complex terrain in the future. Nevertheless, there are major objections with the current status of the manuscript as a scientific paper. The authors need to add a clear scientific objective and rewrite the manuscript following a red line to answer the research question. Therefore, the current knowledge gaps need to be clarified in the introduction, too. The structure of the manuscript needs revision to follow the IMRAD scheme. The figures are well made, some corrections are stated in the specific comments.

The role of the presented simulations is unclear, since they are just introduced briefly and the agreement to the measurements is quite bad. The interesting findings of wind speed differences over the ridges should not just be described in the text but better discussed. The authors should consider to focus on the validation of the lidar scans using the available in situ measurements on the met masts or on improving the simulations on the basis of all presented flow measurements and a realistic forest representation.

We revised the entire manuscript with a focus to clarify the study's objectives and having a clearer structure. The revised manuscript follows now the IMRAD scheme. Please see for details our comments to your specific comments below and the attached marked-up version of the manuscript. Most importantly, we added an entire discussing section focusing on the interpretation of the observations and the role and limitations of the WRF-LES simulation.

Specific comments and technical corrections

1. Better define terms or choose just one for similar meanings: scanning lidar, WindScanner, Multi-lidar, dual-Doppler, etc.

Thanks for this comment. We use now consistently the term “scanning lidar” throughout the manuscript.

2. Please proofread the manuscript on use of times.

We proofread the entire manuscript and corrected the use of times.

3. P2L5, examples for current usage of long range lidar: please precise type of lidar applications, i.e. for single wind turbine wakes no large areas have to be scanned.

Please limit references to some recent papers. Further state of the art applications of scanning long range lidar worth mentioning here are scanning lidar based wind/power forecasts and research on wind farm wakes.

This paragraph has been updated it now reads as follows: "Moreover, many studies utilized the scanning capability to measure wind fields over large areas for wind energy purposes in assessing, for example, wind turbine wakes (Trujillo et al., 2011; Iungo et al., 2013; Bodini et al., 2017; Menke et al., 2018b), the inflow towards wind turbines (Mikkelsen et al., 2013; Simley et al., 2016; Mann et al., 2018), the influence of surface and terrain features on the flow (Lange et al., 2016; Mann et al., 2017) and atmospheric phenomena such as gravity waves (Palma et al., 2019)."

4. *Sec 2.1.1: shorten description of 2015 campaign since not used here. Focus on setup used in this article. Better explain and justify statements made (e.g. laser beams need to be chosen "as low as possible").*

The description of the section now solely focuses on the 2017 campaign.

5. *P4L16: $\cos(5^\circ) \approx 0.996$, please correct.*

Corrected.

6. *Sec 2.1.2: Focus on relevant information. Type of lidar power supply not relevant, limit information to the fact of disturbances in power supply.*

Unnecessary information has been removed from this section.

7. *Fig 1: Please use consistent naming for met masts, lidars, etc. Here lidars are named 105, 106, etc. In Table 1 names are WS5, WS6, etc.*

Corrected. We are referencing the SLs now by the 105, 106, ... convention throughout.

8. *Fig 1: Please add information about the used coordinate system (PT-TM06/ETRS89) in the text.*

The coordinate system is mentioned in the caption of the figure.

9. *Sec 2.1.3: Please shorten description of the networking schemes etc. to the relevant information (offsets and usage of GPS time). Add information on spatial averaging along the scan trajectory resulting from continuous scanning and in beam direction resulting mainly from the pulse length. Basic information like the type of the used lidar systems is missing.*

The description of the network scheme has been shortened and information about spatial averaging and other basic information has been added.

10. P5L6: Please specify descriptions of setup. "Range gates were placed every 10 m along the laser beam ...".

The description of the scanning scenario has been expanded including a definition of the range gate term.

11. P5L15: unit of first numbers missing! 0.42 s pm 1.03 s or (0.42 pm 1.03) s

Corrected.

13. Sec 2.2: Information on humidity sensors mentioned in the manuscript is missing here!

The NCAR SHT75 sensor is a combined temperature and humidity sensor. This information was missing in this section and has been added. Thanks for pointing this out.

14. P5L20: "The 100 m masts also have instruments at 80 and 100 m." What kind of instruments are those? Is this information relevant here?

The instruments at 80 and 100 m are sonic anemometers and temperature /humidity sensors. The data of the sensors at these heights is used in this manuscript and those important to mention. We clarified the instrument type in the manuscript.

15. Sec 3: If you decide to show simulation results please describe the setup in more detail. It is ok to reference to another detailed description, but all basic information needed to understand this work should be included.

We significantly expanded the description of the simulation. Please find the changes in the attached marked up version of the manuscript.

16. P6L17-19: Move information on data availability to section "Data availability"

The information has been moved to the "Data availability" section. Thanks for pointing this out.

17. P6L21: Please describe the vertical coordinate system and relate it to the coordinates used for lidar data and simulation data.

The coordinate system has been specified. The manuscript reads now as follows: "The anemometer data are rotated into a vertical coordinate system (i.e. w is aligned with the vertical axis of the local coordinate, PT-TM06/ETRS89, system which is also used for the lidar data) and oriented to true North from angles determined by laser multistation scans of each instrument."

18. Sec 4.2.1: Has the filter method used here been introduced before? Has it been validated? Is the assumption of the "certain degree of continuity" of the atmosphere and are the chosen thresholds appropriate here? In Figure 2 this approach is called

“dynamic filtering approach”. Please use consistent naming. Why is the approach dynamic when thresholds are static and chosen manually?

To our knowledge, this filtering method has not been introduced before. However, it is based on a similar, less complex filtering approach that was developed for a different lidar dataset that has been not been published. The thresholds and the underlying assumption of continuity in the wind field have been intensely tuned and tested for the present dataset and has been found to work well in different atmospheric conditions. Different approaches, without success, have been tested to remove fixed thresholds from the method. The use of the term “dynamic” was taken up as the filtering method, due to its running averages windows, adjusts to certain parts of the measured wind field. We agree that the term can be misleading and removed it from the manuscript.

19. Fig 2: Labels a), b) etc. are missing. b) is called “filtered data” in the title and “dynamic filtering approach” in the caption. The order of c) and d) is swapped in the caption. Please correct.

The figure has been corrected.

20. Sec 4.3: The information from this short section should be moved to Sec. 3.

The section has been integrated into section 3 as suggested.

21. Sec 5.1: This section is said to contain results but starts with methods (c.f. comment on IMRAD-structure above).

Thanks for this comment. We moved the description of methods from this section to section 4.1.

22. Fig 4: Please specify lidars used for single subplots.

The lidars are now specified in the caption of the figure.

23. Fig 4: U_hor and U_proj not introduced in the text. Markers and fits could not be distinguished.

U_hor and U_proj are introduced in section 4.1. The markers are indeed difficult to distinguish as the difference between U_hor and U_proj is neglectable what we are highlighting here.

24. Sec 5.2: Findings described are not referenced to the relating figure.

The findings described in section 5.2 are not shown in any figure that is part of the manuscript. We added a note specifying this to the manuscript.

25. P11L7: Please move methodology for the retrieval of atmospheric stability to methods section.

Thanks for this suggestion. The content has been moved to section 4.1.

26. *Fig 5: Please define N, u and elev given in the plots.*

The definitions have been added.

27. *Fig 6: Different line styles are suggested for both WRF conditions to support readability in black and white printing.*

The line styles have been changed to improve the black and white printing readability.

28. *P16L28: Calling the aerial laser scanner measurements “lidar” might confuse the reader. Please distinguish between the terms for wind lidar and lidar for distance measurements.*

The term “aerial laser” is now consistently used when referring to lidar distance measurements.

29. *P16L25 and following: It could be expected that numerical simulations without forest parametrization and with a non-realistic forest parametrization will lead to poor results. I suggest simulations with a realistic forest parametrization or excluding simulations with a change of the focus of the manuscript (see comment above).*

Generally, forest is considered in simulations by increasing the surface friction in forested areas and special forest parameterization is not considered as a standard method. Thus, using a simulation without specific forest drag parametrization can be considered as a reference case. In our view, it is not obvious which result can be expected from either of the two simulations. Even though the forest height in the simulation with parametrization is too high, we could show that the correlation of simulation results and measurements has been improved which can be valuable for future simulation setup. Due to limited resources, we are unfortunately not able to perform further simulations.

30. *Sec 6: The major part of this section is a summary, not a conclusion. Please rewrite.*

The conclusion section has been entirely rewritten. Please find the updated version in the attached marked up version revised manuscript.

Multi-lidar wind resource mapping in complex terrain

Robert Menke¹, Nikola Vasiljević¹, Johannes Wagner², Steven P. Oncley³, and Jakob Mann¹

¹Technical University of Denmark - DTU Wind Energy, Frederiksborgvej 399, 4000 Roskilde, Denmark

²Deutsches Zentrum für Luft- und Raumfahrt, Institut für Physik der Atmosphäre, 82234 Oberpfaffenhofen, Germany

³National Center for Atmospheric Research, Earth Observing Laboratory, Boulder, CO, USA

Correspondence: Robert Menke (rmen@dtu.dk), Jakob Mann (jmsq@dtu.dk)

Abstract. Scanning Doppler lidars have great potential for reducing uncertainty of wind resource estimation in complex terrain. Due to their scanning capabilities, they can measure at multiple locations over large areas. We demonstrate this ability ~~using with~~ dual-Doppler lidar measurements of flow over two parallel ridges. The data have been collected using two pairs of ~~long-range WindScanner systems scanning lidars~~ operated in a dual-Doppler mode during the Perdigão 2017 measurement campaign. ~~The~~ There the scanning lidars mapped the flow ~~along the southwest and northeast ridges~~ 80 m above ground level ~~along two ridges, which are considered favorable for wind turbine siting. The measurements are validated with sonic wind measurements at each ridge.~~ By analyzing the collected data, we found that ~~for different flow conditions on average~~ wind speeds are ~~on average~~ 10% higher over the southwest ridge compared to the northeast ridge. At the southwest ridge, the data shows, ~~depending on the atmospheric conditions~~ for approach flow normal to the ridge, a change of 20% in wind speed along the ridge. ~~Fine differences like these are difficult to reproduce with computational flow model as we demonstrate by comparing the lidar measurements with Weather Research and Forecasting LES (WRF-LES) simulation results.~~ For the measurement period, we have simulated the flow over the site using WRF-LES to compare how well the model can capture wind resources along the ridges. We used two model configurations. In the first configuration, surface drag is based purely on aerodynamic roughness whereas in the second configuration forest canopy drag is also considered. We found that simulated winds are underestimated in WRF-LES runs with forest drag due to an unrealistic forest distribution on the ridge tops. The correlation of simulated and observed winds is, however, improved when the forest parameterization is applied. WRF-LES results without forest drag overestimated the wind resources over the southwest and northeast ridges by 6.5% and 4.5% respectively. Overall, this study demonstrates the ability of scanning lidars to map wind resources in complex terrain.

1 Introduction

Traditionally, wind resource assessment is done with mast-mounted cup or sonic anemometers. Nowadays, with the commercialization and increasing acceptance of remote sensing devices such as lidars and sodars, this practice is changing due to clear advantages of remote sensing devices: they are easily deployed, ~~easier~~ ~~can be cost-effective~~, avoid the requirement of building permits, and can measure at higher heights. However, mast based instruments, especially sonic anemometers, are probably still better suited for turbulence measurements (Sathe and Mann, 2013).

Vertically profiling wind lidars gained popularity for the assessment of mean wind speeds and are getting recognized by international standards for wind resource and power performance assessments (Clifton et al., 2018). Most profiling lidars perform velocity–azimuth display (VAD) scans to estimate the horizontal velocity from line-of-sight (LOS) measurements under the assumption of horizontal homogeneity. However, this assumption is typically violated in complex terrain. Errors from profiling 5 lidars can be up to 10% when measuring in complex terrain as shown by Bingöl et al. (2009). One solution to overcome this problem is to use several lidars that directly measure different components of the wind at the same location. Moreover, the deployment of several lidars with scanning capabilities allows the assessment of wind conditions over large areas (Vasiljević et al., 2019) which can give important insights into the spatial variability of flow over very complex terrain. Multi-lidars have been proven to have a high measurement accuracy in comparison studies with sonic anemometers (Pauscher et al., 2016). Moreover, 10 many studies utilized the scanning capability to measure wind fields over large areas for wind energy purposes in assessing, for example, wind turbine wakes (Bingöl et al., 2010; Käsl er et al., 2010; Trujillo et al., 2011; Jungo et al., 2013; Bodini et al., 2017; Menke et al., 2018), the inflow towards wind turbines (Mikkelsen et al., 2013; Simley et al., 2016; Mann et al., 2018), the influence of surface and terrain features on the flow (Lange et al., 2016; Mann et al., 2017) and atmospheric phenomena such as gravity waves (Lechner et al., 2016; Palma et al., 2019)(Palma et al., 2019).

15 In this publication, we will present use measurements from the Perdigão 2017 campaign (Fernando et al., 2019). For this measurement campaign, wind lidars were a key measurement technology for the assessment of the flow over the complex terrain site. In total 7 profiling and 19 scanning lidars (SL) were deployed. The present study focuses on a subset of the entire data collection containing measurements of wind resources along the two parallel ridgestwo ridges, which are favorable sites for wind turbines, at the Perdigão site.

20 The relevance of such measurements is especially important for complex terrain sites where the uncertainty of current flow models is high (Bechmann et al., 2011). Potential sources of error are the characterization of the roughness resulting from different types of canopies (Wagner et al., 2019a), the characterization of the stratification in the atmosphere (Palma et al., 2019), the description of the terrain (Lange et al., 2017; Berg et al., 2018) and model resolution which may not capture all important flow phenomena in complex terrain. We compare our measurements Therefore creating a good measurement dataset of the flow over such terrain is imperative to improve the models. In this study, we present dual-Doppler lidar measurements and analyze flow structures in observed wind field for different atmospheric conditions. Moreover, the lidar measurements are compared to a WRF-LES simulations with and without a parametrization of forest drag (Wagner et al., 2019a, b) to test the model capability in reproducing the observed flow structures.

25 This-The paper is organized in the following way: Section 2 gives an overview of the Perdigão field campaign including a description of lidar and mast measurements, Section 3 presents the WRF model setup. Section 4 introduces the applied data processing techniques. The results and discussion of the data analysis are given in sectionSection 5, followed by our conclusions in seetionSection 6.

2 Field campaign overview

The Perdigão 2017 field campaign took place at a site centered at the village Vale do Cobrão located in Portugal close to the Spanish border. The main selection criteria for the site was a distinct terrain feature of two parallel ridges of 4 km in length (Figure 1). The ridges are about 1.5 km apart and the height difference from the valley bottom to the ridge tops is about 250 m.

- 5 The northwest – southeast orientation of the ridges is perpendicular to the prevailing wind directions which were assessed previously to the campaign with a 30-m measurement mast (Vasiljević et al., 2017).

During the 2017 campaign, measurement devices were set up with a very high density by a large international group of universities, [research](#) institutions and industry partners. Instruments were operated from early 2017 until early 2018 with an Intensive Operation Period (IOP) from May 1st to June 15th 2017. To map the flow over the measurement site 186 3-
10 component sonic anemometers were installed on 50 meteorological masts with heights up to 100 m. Also, 26 wind lidars (7 profiling lidars and 19 scanning lidars) were deployed. A full overview of the campaign's objectives and instrumentation may be found in Fernando et al. (2019). For this study, we analyze measurements from 4 [long-range WindScanners lidars](#) ([Vasiljević et al., 2016](#)) [SLs](#) and 4 measurement masts located on the ridge tops.

2.1 Lidar measurements

- 15 As mentioned above, for this study we analyze measurements of four out of the eight [WindScanners SLs](#) that were operated by DTU during the measurement campaign. [Specifically, we are focusing on a measurement scenario designed to measure the wind resources along the two ridges which was achieved using the so-called ridge scans \(Vasiljević et al., 2017\)](#) The SLs, of type Leosphere 200s, were operated as WindScanners (Vasiljević et al., 2016). The WindScanner specific modifications allow to measure complex trajectories and the synchronization of multiple systems. In the following sections we will describe the
20 experiment layout design process, the deployment process including the calibration procedure, and the design and configuration of the scanning trajectories.

2.1.1 Layout

[The layout of the 2017 experiment is an extension of the design introduced in the 2015 pilot Perdigão experiment \(Vasiljević et al., 2017\).](#)

- In 2015, our focus was to measure wind resources above the southwest (SW) ridge using a single pair of WindScanners
25 and the northeast (NE) ridge since the ridge tops are areas characterized with high wind resources and thus often used as locations for wind turbines turbine placement in complex terrain. [Also, current state-of-the-art flow models have difficulties predicting the flow behavior over the steep ridges. Therefore creating a good measurement dataset of the flow over such terrain is imperative to improve the models.](#)

- In 2015 we established a traverse line. Accordingly, a measurement scenario was designed probing wind resources above both
30 ridges. The scanning scenario, the so called ridge scan, of intersecting lidar beams along transect following the SW and NE ridge for about 2 km in length along the SW ridge 80 m above the ground level (AGL). [This altitude was is designed \(Figure 1\).](#) This layout presents an extension of the design of the 2015 campaign (Vasiljević et al., 2017). The altitude of 80 m is chosen to

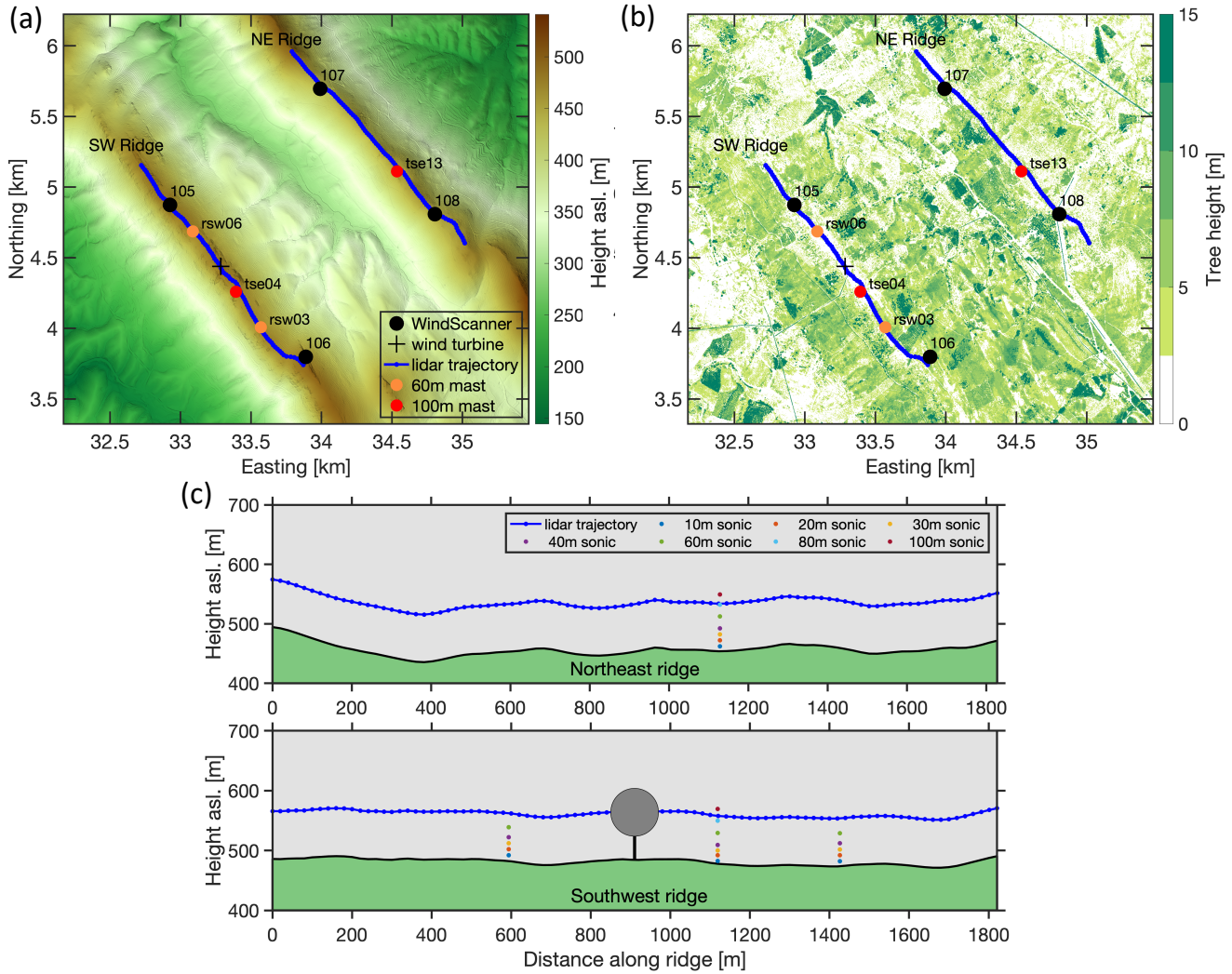


Figure 1. (a) Elevation map of the Perdigão site in the PT-TM06/ETRS89 coordinate system. (b) Tree height map. (c) View from the southwest of the ridges with lidar and sonic anemometer sampling positions, and wind turbine at center of the southwest ridge.

match the hub height of the wind turbine located on the SW ridge. With only a pair of lidars used to measure along each ~~traverse line~~^{transect}, it is not possible to resolve the vertical velocity component. Thus, the lidar positions and scan strategy needed to be chosen to keep the elevation angles of the laser beams as low as possible (preferably below 5°). Also, the intersecting angle between the laser beams must be at least 30° . Having elevation angles below 5° ensures that the influence of the vertical wind component is kept below 0.5% as $\cos(5^\circ) = 99.6$. In 2015, we placed a single pair of WindScanners on the northeast (NE) ridge, bringing them close the height of the traverse above the SW ridge to keep the elevation angles low. The separation of the WindScanners was about 1.2 km to match the design conditions for intersecting angles (Vasiljević et al., 2017). For the 2017

campaign, we extended our goal by also placing WindScanners on the SW ridge, thus enabling simultaneous probing of wind resources above both ridges (Figure 1). The in-field placement of the lidars was done using is based on high precision terrain data and orthophotos acquired prior to the Perdigão 2015 campaign (Vasiljević et al., 2017).

2.1.2 Deployment

5 The Perdigão site is rural, characterized by rugged terrain accessible with a limited off-road route network. Actually, the network had to be extended to allow access to several instruments. In 2015, the WindScanners were powered by a diesel generator, whereas in 2017 a dedicated power grid was constructed to supply uninterrupted power to the devices. For these reasons, the initial deployment of instruments was complicated and time-consuming.

10 After the WindScanners After the SLs were positioned at their designated locations, their orientation and leveling were determined by mapping the lightning rods of measurement masts using the WindScanners SLs' laser beams (Vasiljević, 2014, p.157). Both the position of WindScanners SLs and lighting rods had been measured with centimeter accuracy (Menke et al., 2019a). By comparing referenced and mapped positions the leveling and orientation of WindScanners SLs were improved resulting in a pointing accuracy of about 0.05° . To retain the pointing accuracy, the target mapping was repeated several times during the campaign to ensure that the leveling and orientation of the WindScanners SLs remained unchanged.

15 2.1.3 Scanning strategy

The two traverses trajectories, which follow the ridge top line 80 m AGL, were designed using the high precision terrain data. The traverses were 1.8 km long and described by points evenly spaced every 20 m. Accordingly we programmed the WindScanners SLs to measure continuously along the traverses trajectories by moving the beams through the traverse trajectory points with the speed of 40 m s^{-1} and an accumulation time of 500 ms. As a result, spatial averaging takes place normal to the beam direction. Along the beam, range gates were placed every 10 m, starting at 700 m, and extending to 2640 m (Table 1). Range gates are time intervals used to determine the wind speed from the back-scattered light. Each range gate corresponds to a spatial interval for which the radial velocity is evaluated. In our case, this translates into a weighting function with a full-width half maximum of about 30 m. One scan took 48 s of which 45 s were spent on measurements, 0.5 s for acceleration and deceleration of the scanner heads and 2 s to return to the trajectory start point. Range gates were placed every 10 m, starting at 700 m, and extending to 2640 m (Table 1).

Typically, the WindScanner system uses a master computer to keep the synchronization of WindScanners SLs to about 10 ms (Vasiljević et al., 2016). This synchronization requires a stable network connection between the WindScanners SLs and the master computer. At the Perdigão site the systems were connected via directional long-range WiFi antennas which had tendency to have a low availability and/or high latency. Due to, due to the unstable network the WindScanners conditions, the SLs were configured to start the measurements in a scheduled fashion according to GPS time, thus independently from the master computer. This introduced time offsets due to a system dependent startup time which varies over time and among the different WindScanners SLs. However, the WindScanners SLs could perform measurements independent of the network

connection which results in higher data availability. The average time offset between ~~WS5 and WS6~~ ~~SL 105 and 106~~ is 0.42 ± 1.03 s and 0.7 ± 0.65 s between ~~WS7 and WS8~~ ~~SL 107 and 108~~.

Table 1. ~~WindScanner~~ Scanning lidar coordinates and details about the measurement settings.

WindScanner Scanning lidar	105	106	107	WS8 -108
northing (m)	32926.47	33888.66	33990.61	34804.57
easting (m)	4874.29	3798.01	5695.30	4807.90
elevation (m)	485.94	486.34	437.06	452.81
azimuth range ($^{\circ}$)	38.54 - 97.36	357.39 - 54.45	246.88 - 183.48	279.43 - 221.17
mean elevation ($^{\circ}$)	1.83	1.79	4.71	3.80
range gates	195 (from 700 m every 10 m up to 2640 m)			
accumulation time (ms)	500			
pulse length (ns)	200			

2.2 Mast measurements

For this study, we use measurements from four masts. One 100 m mast was located on the NE ridge and a 100 m and two 60 m masts that were located on the SW ridge. All masts are equipped with 3-D ultrasonic anemometers (Gill WindMaster Pro) and temperature/relative humidity sensors (NCAR SHT75) at the heights of 10, 20, 30, 40 and 60 m AGL and 2, 10, 20, 40 and 60 m AGL, respectively. The 100 m masts also have instruments-ultrasonic anemometers and temperature/relative humidity sensors at 80 and 100 m AGL. Data were acquired at 20 samples per second with a $1 \mu\text{s}$ resolution GPS-based time stamp on every sample.

10 3 Flow modeling overview

In this study, long-term simulations of Wagner et al. (2019a, b) are compared to lidar ridge scans to determine the quality of a numerical model over complex terrain. Model simulations were performed with the Weather Research and Forecasting (WRF) model (Skamarock et al., 2008) on three nested domains D1 to D3 with horizontal resolutions of 5 km, 1 km, and 200 m, respectively. The innermost domain D3 is run in large-eddy simulation (LES) mode. The LES set-up was chosen to be independent of boundary layer parameterizations in domain D3, although a horizontal resolution of 200 m is relatively coarse for a LES run. Vertical nesting is applied to define individual levels in the vertical for each model domain. For domains D1–D3, 36, 57 and 70 vertically stretched levels are used and the respective lowest model levels are set to 80, 50 and 15 m above ground level. The model top is defined at 200 hPa (about 12 km height) to include radiation and cloud effects at the tropopause. At the model top, a 3 km thick Rayleigh damping layer is applied to prevent wave reflection. The simulation is initialized once

at 00:00 UTC on 30 April 2017 and run for 49 days and 18 h until 18:00 UTC on 18 June 2017. The initial and boundary conditions are supplied by European Centre for Medium-Range Weather Forecasts (ECMWF) operational analyses on 137 model levels with a horizontal resolution of 8 km and a temporal resolution of 6 h. The WRF output interval of domain D3 was set to 10 min. The complete model setup including the physical parameterizations that were used is described in detail in

- 5 Wagner et al. (2019a) and in Wagner et al. (2019b). Two simulations were performed for the whole IOP of the Perdigão 2017 campaign and are run with (WRF_F) and without (WRF_NF) a forest parameterization in the LES domain D3. Without forest parameterization, surface drag is defined by an aerodynamic roughness length z_0 , which is obtained from the CORINE 2012 land-use data set and converted to land-use types according to Pineda et al. (2004). In the WRF_F run, an additional forest drag term following Shaw and Schumann (1992) is implemented, which decelerates the flow on the lowermost model levels. The
10 forest cover and leaf area index (LAI) are retrieved from the CORINE data set. As no information, at the point of the model configuration, about the tree height was available, for the modeling domains, a randomly uniformly distributed forest height of 30 m \pm 5 m was used. The high resolution aerial scans are only available for a smaller area centered around the measurement site (Figure 1b). A detailed description of the forest parameterization and the differences between the WRF_F and WRF_NF simulations is given in Wagner et al. (2019b).

15 **4 Data overview**

In the following, data processing methods for the mast, lidar and WRF-LES datasets are described. The measurement datasets are publicly available. The lidar data can be obtained from Menke et al. (2018a) and mast data is available via the NCAR archive in 5 minute and 20 Hz resolution (UCAR/NCAR – Earth Observing Laboratory, 2019a, b). Model data of the LES domain D3 is available with a 10 minute output interval. This means that every 10 minutes a snapshot of the simulated meteorological
20 condition is written to the output file. The three-dimensional fields are interpolated linearly in both the horizontal and vertical direction to the lidar ridge scan coordinates. This results in time series of meteorological variables at each lidar scanning point, which can be compared to lidar data.

4 Data overview and processing methods

4.1 Mast data

- 25 The anemometer data were are rotated into a vertical coordinate system (i.e. w is aligned with the vertical axis of the local coordinate, PT-TM06/ETRS89, system which is also used for the lidar data) and oriented to true North from angles determined by laser multistation scans of each instrument. No issues were are determined in the quality control process, so the reported data from the anemometers have been is used unedited.

The fans used to aspirate the temperature/relative humidity sensors on the masts occasionally failed during the project. Data
30 from these periods were removed. Also, for some of these sensors, laboratory post-experiment calibrations indicated larger than

expected differences from the pre-calibrations (usually less than 0.5 degC and 4%RH). For these sensors, the post-calibrations ~~were~~are applied.

For the comparison of sonic and lidar measurements, we project the 80 m sonic wind speeds to the SL LOSs using equation 1 and calculate the sonic wind speed projected to the plane spanned by the two lidars. The former is calculated as,

5 $V_{r_sonic} = u \sin \phi \cos \vartheta + v \cos \phi \cos \vartheta + w \cos \vartheta$ (1)

where V_{r_sonic} is the sonic wind speed projected to the individual LOSs of the SLs and u , v and w are the wind vector components. The sonic data are averaged exactly during the accumulation period (500 ms) of the SLs at the two closest range gates to the masts that are not affected by the measurement mast structures. These range gates are about 40 m to NW (northwest) and SE (southeast) of the masts.

10 The latter, the sonic wind speed projected to the plane spanned by the two lidars, is used to investigate the correlation of horizontal wind speeds measured by the sonics and the lidars. For the sonic measurements we consider the horizontal wind speed ($U_{hor} = \sqrt{u^2 + v^2}$) and the wind speed projected to the plane spanned by the two lidars ($U_{proj} = \sqrt{u_{proj}^2 + v_{proj}^2}$). Where the projected wind vector is calculated as:

$U_{proj} = \mathbf{n} \times (\mathbf{U} \times \mathbf{n})$ (2)

15 with \mathbf{n} being the unit normal vector of the plane spanned by the two lidar beams.

Furthermore, the mast data is used to determine the atmospheric stability based on the Richardson number (Ri) calculated at the upstream mast as defined in Menke et al. (2019b) based on the potential temperature gradient from 20 m to 100 m and the 100 m wind speed. It is not obvious how to define limits for different stability regimes thus we define stable conditions as periods with $Ri > 0$ and unstable conditions as $Ri < 0$. Neutral conditions are only expected to occur during short transition

20 periods.

4.2 Lidar data

We process the lidar data in three consecutive steps. First, the data are filtered using the method described in section 4.2.1. Next, the measurements of the filtered scans along the ridge trajectories are combined to horizontal winds, see section 4.2.2. Finally, the combined measurements are averaged over 10 minute periods.

25 **4.2.1 Filtering**

Most commonly, lidar data are filtered by thresholding using the carrier-to-noise ratio (CNR) as a quality indicator. These methods are described by Beck and Kühn (2017) who give a general overview of lidar data filtering approaches and also present highly innovative methods. Here we are proposing a new approach which is based on the assumption that the wind field has a certain degree of continuity. We filter the lidar data in a three-stage process that is applied to each scan: In stage 30 one, the data are filtered based on a moving median value of the LOS velocities measured along each LOS. The median is

calculated for a window that stretches over 15 range gates corresponding to a distance of 150 m. All range gates that deviate by a threshold of 3 m s^{-1} from the median are excluded.

- In stage two, all measurements that exceed the median of radial velocities along an entire LOS by a threshold value of 6 m s^{-1} are filtered out. Both thresholds were determined by visual inspections of plotted data and tuned to the present values.
- 5 After each stage, missing range gates are linearly interpolated by the value of the two neighboring range gates in case they have valid values. In a final stage, range gates with valid values that are surrounded by three or more invalid range gates out of the two previous and two following range gates are excluded. These range gates are considered as scatter that are unlikely to have a valid measurement or have a meaningful contribution to the analysis. The first two stages are intended to remove local and global artifacts in the measurements. Finally, all filtering stages are repeated across LOSs in the azimuthal direction.
- 10 We demonstrate the performance of this method compared to CNR filters with the thresholds of -24 dB and -27 dB (Figure 2). Our approach recovers more data in the far range of the scans thus extends the range of the scans during periods with low CNR and can remove artifacts caused by e.g. hard targets or second return pulses originating from, for example, a cloud base at a higher elevation. The average availability with our [dynamic filtering](#) approach is 91.8% compared to 77.7% (92.2%) with a -24 dB (-27 dB) filter. The high availability of the -27 dB filter is misleading in the sense that this method does not remove all
- 15 artifacts from the scans (compare Figure 2c).

4.2.2 Wind vector reconstruction

The horizontal components of the wind vector (u positive east and v positive north) are reconstructed from measurements of the two [WindScanners-SLs](#) measuring along the same ridge. The measurements at the 92 ridge trajectory points are combined applying equation 3:

$$20 \quad \begin{bmatrix} u \\ v \end{bmatrix} = \begin{bmatrix} \sin \phi_1 \cos \vartheta_1 & \cos \phi_1 \cos \vartheta_1 \\ \sin \phi_2 \cos \vartheta_2 & \cos \phi_2 \cos \vartheta_2 \end{bmatrix}^{-1} \cdot \begin{bmatrix} V_{r1} \\ V_{r2} \end{bmatrix} \quad (3)$$

with V_r being the radial or LOS velocities measured by the two [WindScanners-SLs](#), ϕ the azimuth angles using the geographical convention, i.e. 0° is pointing north and ϕ increases clockwise, and ϑ the elevations angles of the scanners. In this calculation the influence of the vertical wind component w is considered to be negligible since we measured at low elevation angles. We combine 10-minute averaged radial velocity components. Measurement points with less than 10 independent samples are disregarded as well as complete scans with more than 20% invalid data.

4.2.3 Data availability

The four [WindScanners-SLs](#) operated for different periods from March 22 to July 24. Individual system availability in these periods range from 59% to 80% (Table 2). During the IOP, due to the permanent presence of people at the site to aid in the case of a power grid or system failures, the [WindScanners-SLs](#)' availability is higher (71% to 92%). For dual-Doppler retrievals 30 at the individual ridges, concurrent availability of WS5 and WS6 for the NE ridge and WS7 and WS8 for the SW ridge is

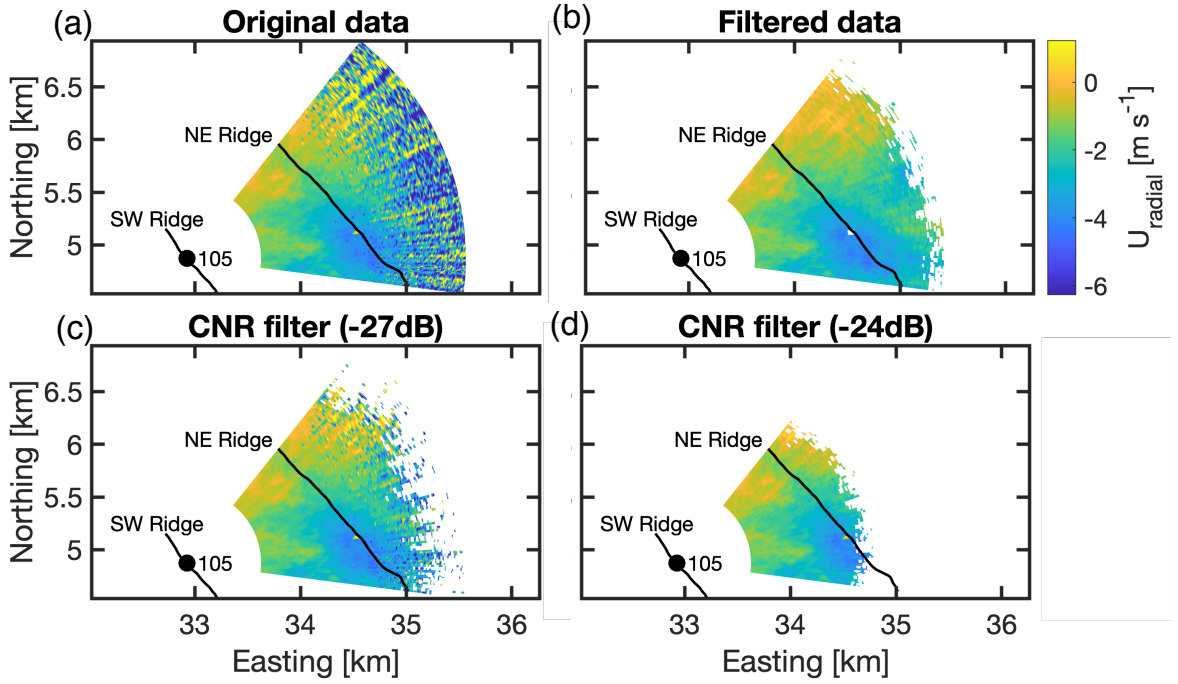


Figure 2. Comparison of data recovery with different filters for the 10 minute period starting at May 03, 2017 13:40 UTC. a) unfiltered data, b) dynamic filtering filter data following the approach described in section 4.2.1, c) -24–27 dB filter, and d) -27–24 dB filter.

required. The combined availability during the IOP is 79% and 51% for the NE and SW ridge, respectively. Simultaneous measurements at both ridges are available for 44% of the period of the IOP. After applying filtering processes as explained in section 4.2.1, the data availability reduces to 31.6%. When wind speeds are also required to be above For the analysis, we only use measurements of the IOP period, due to the higher data availability, and removed periods with wind speeds below 3 m s^{-1} at 80 m height (measured at the mast tse04) which leaves 507 10 minute periods are left for the analysis, corresponding to 23% of the IOP period.

4.3 Flow model data

Model data of the LES domain D3 is available with a 10 minute output interval. This means that every 10 minutes a snapshot of the simulated meteorological condition is written to the output file. The three-dimensional fields are interpolated linearly in both the horizontal and vertical direction to the lidar ridge scan coordinates. This results in time series of meteorological variables at each lidar scanning point, which can be compared to lidar data.

Table 2. Operation time and data availability of WindScanners SLs. Number in brackets is the number of available 10 minute periods.

WindScanner Scanning lidar	105	106	107	WS8-108		
start of operation	March 27, 16:50	March 27, 16:50	March 22, 17:50	March 27, 16:50		
end of operation	June 17, 15:20	June 17, 09:50	July 10, 16:50	July 24, 15:50		
scanner availability	72.8% (2863)	79.8% (3130)	58.6% (3094)	63.2% (3608)		
scanner availability IOP	82.2% (1815)	91.6% (2023)	70.7% (1562)	77.0% (1701)		
combined availability IOP (per ridge)	NE ridge 79.3% (1751)		SW ridge 51.3% (1133)			
combined availability IOP (both ridges)	44.2% (976)					
combined availability IOP (after filtering)	31.6% (698)					
combined availability IOP (after filtering, $U > 3 \text{ m s}^{-1}$)	23.0% (507)					

5 Data analysis

5.1 Comparison of mast and lidar measurements

The correlation of radial velocities measured by the individual WindScanners SLs and of the reconstructed wind vectors with the sonic wind speeds is calculated. We project the 80 m sonic wind speeds to the lidar LOSs using equation 1.

$$5 \quad V_{r\text{-sonic}} = u \sin \phi \cos \vartheta + v \cos \phi \cos \vartheta + w \cos \vartheta$$

The sonic data are averaged exactly during the accumulation period (500 ms) at the two closest range gates to the masts that are not affected by the measurement mast structures. These range gates are about 40 m to NW (northwest) and SE (southeast) of the masts. For all WindScanners For all SLs the correlation coefficient for the LOS measurements are better than 0.994, offsets are less than 0.45 m s^{-1} and slopes deviate by less than 0.04 from 1 (Figure 3). Considering that the measurements are not collocated and that the measurement volumes of lidars and sonics differ by about two orders of magnitude these correlations can be considered as good. For this comparison, only measurements from IOP are selected, and measurements are limited to the prevailing wind directions ($\pm 15^\circ$ centered around the transect orientated 54° towards north) to eliminate the effects of mast wind shadow and to be consistent with the data fraction used for the further analysis.

The correlation based on the reconstructed wind vectors is calculated for 10-minute averages at all four mast . For the sonic measurements we consider the horizontal wind speed ($U_{\text{hor}} = \sqrt{u^2 + v^2}$) and the wind speed for horizontal wind speeds and wind speeds projected to the plane spanned by the two lidars ($U_{\text{proj}} = \sqrt{u_{\text{proj}}^2 + v_{\text{proj}}^2}$). Where the projected wind vector is calculated as:

$$U_{\text{proj}} = \mathbf{n} \times (\mathbf{U} \times \mathbf{n})$$

with \mathbf{n} being the unit normal vector of the plane spanned by the two lidar beams.

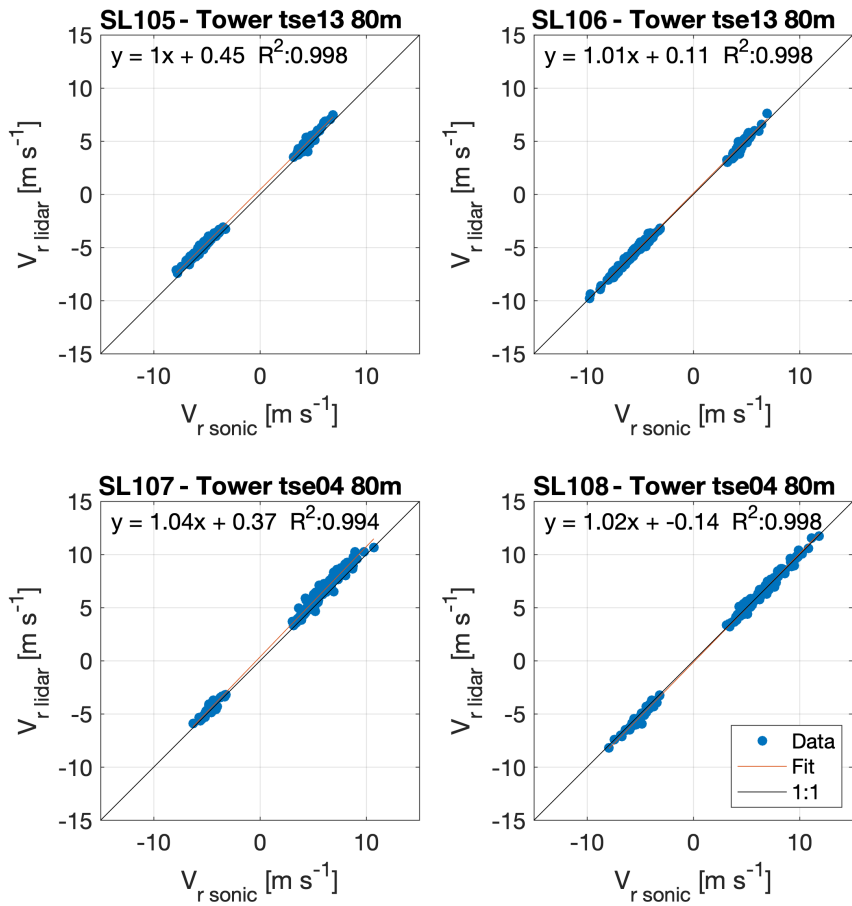


Figure 3. Correlation of radial lidar wind speeds with the sonic wind speeds projected to the lidar LOSs. Only southwesterly and northeasterly wind directions are selected for sectors of $\pm 15^\circ$ centered around the transect orientated 54° towards north.

The Both correlation coefficients with the two 80 m sonics are both better than 0.94, with offsets smaller than 0.25 m s^{-1} and slopes close to 1 (1.04 at tower tse04 and 0.94 at tower tse13, Figure 4). At the 60 m masts the correlation of lidar and sonic measurements is lower due to the spatial difference in height. The correlation coefficients at both masts are 0.9. Differences in the correlations of using the

- Overall, the comparison aids as validation of the lidar measurements. However, the measurements cannot be compared to studies that were designed to directly compare sonic and lidar measurements as e.g. done by Pauscher et al. (2016). Moreover, the correlation of reconstructed wind speeds is the present study shows that differences when comparing the lidar wind speeds to the projected or the horizontal sonic winds speeds are negligibly small. This affirms the decisions made in the design process of the scanning strategy.

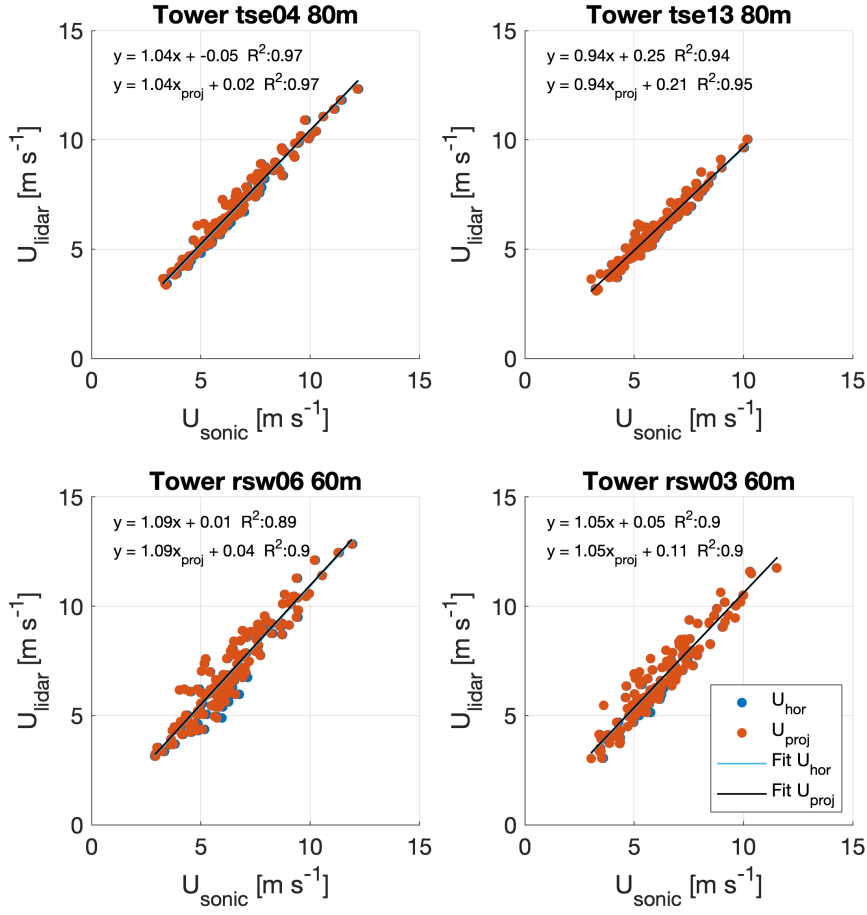


Figure 4. Correlation of reconstructed lidar wind speeds with the horizontal sonic wind speeds and the sonic wind speeds projected to the plane spanned by the lidars. Only southwesterly and northeasterly wind directions are selected for sectors of $\pm 15^\circ$ centered around the transect orientated 54° towards north. Wind speeds at tse04, rsw06 and rsw03 are derived from the SLs 107 and 108, and at tse13 from the SLs 105 and 106.

5.2 Observed flow patterns

Considering all available ridge scan periods (507) we find that the mean wind speed is 10% higher at the SW ridge. Relative changes in wind speed along the SW ridge are below 2%. At the NE ridge, the lowest relative wind speeds are found at the terrain dip at 400 m and a change of 7% in mean wind speed is found along the ridge (not shown). This picture changes significantly during specific atmospheric conditions which are analyzed in the following subsections. We segregate the data by the prevailing flow directions from the northeast and the southwest for sectors of $\pm 15^\circ$ centered perpendicular to the ridge, orien-

tated at 54°(geographical convention). Furthermore, the data are segregated by the atmospheric stability characterized by the Richardson number (Ri) calculated at the upstream mast as defined in Menke et al. (2019b) based on the potential temperature gradient from 20 m to 100 m and the 100 m wind speed. It is not obvious how to define limits for different stability regimes thus we define stable conditions as periods with $Ri > 0$ and unstable conditions as $Ri < 0$. Neutral conditions are only expected to occur during short transition periods.

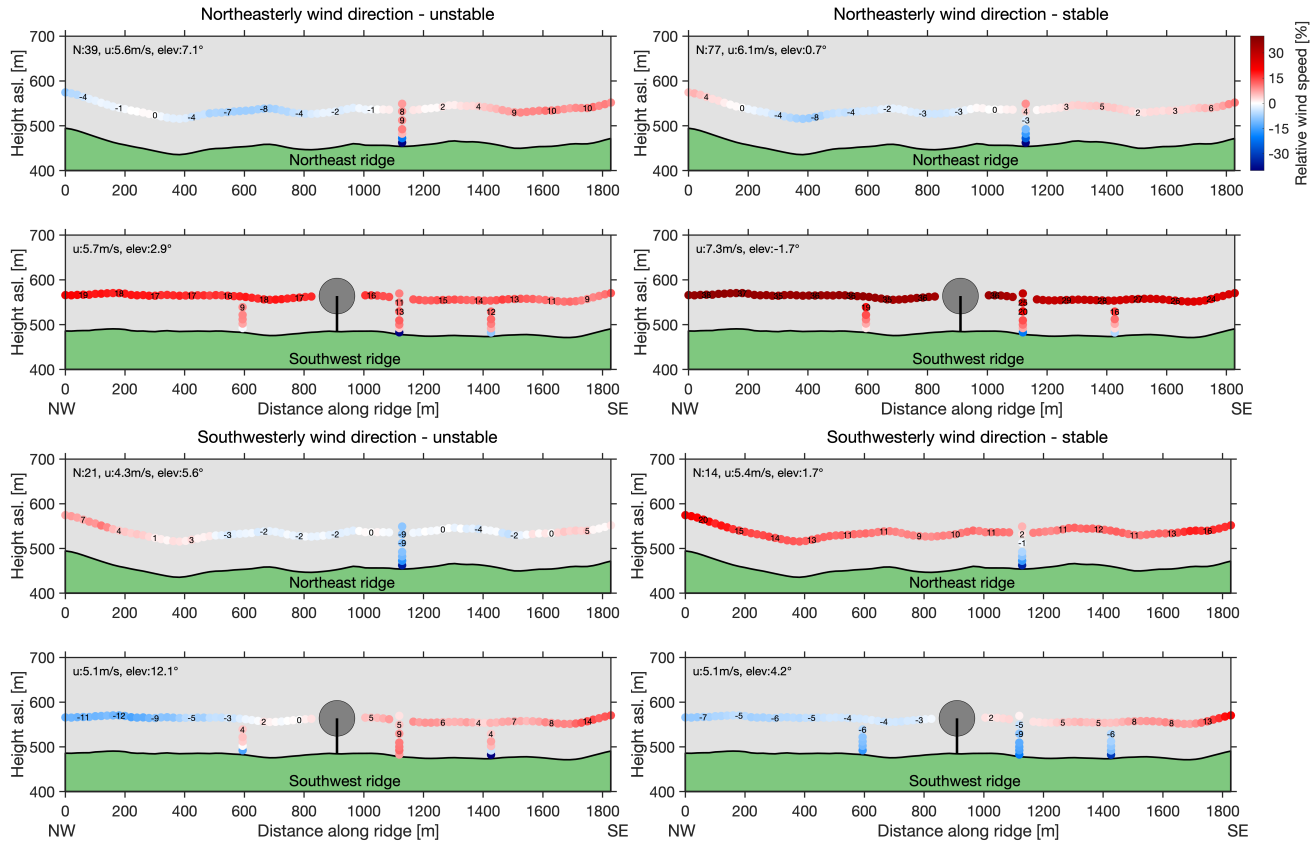


Figure 5. Normalized wind speeds measured by the lidars and sonics during different atmospheric conditions. The wind speeds are normalized by the mean along the upstream ridge e.g. for southwesterly wind directions all measurements are normalized with the mean wind speed along the SW ridge. *N* number of 10-minute periods, *u* horizontal wind speed measured by the 80 m sonic anemometer, *elev* flow elevation angle measured by the 80 m sonic anemometer.

5.2.1 Dependence on wind direction

For southwesterly flows, an increase of more than 20% in relative wind speeds is observed along the SW ridge with higher wind speeds in the southeast (SE) and lower wind speeds in the northwest (NW) (Figure 5). At the NE ridge, for southwesterly

flow, increased relative wind speeds of up to 13% are observed at the NW end of the ridge where the elevation is increasing. All values are relative to the mean wind speed along the upstream ridge.

For northeasterly flow, significantly higher wind speeds of about 25% are observed at the SW ridge. Additionally, a change in wind speed along the SW ridge is observed with higher speeds in the NW and lower in the SE which is opposite to the 5 observation under southwesterly flow. For some conditions, the change in relative wind speed is higher than 20%.

We considered these observations as statistically significant as the mean of standard deviations calculated at each point along the ridge is much lower than the observed changes (Table 3).

5.2.2 Dependence on atmospheric stability

It is most notable that wind speeds at the downwind ridge are always higher than at the upstream ridge during stable conditions 10 (Figure 5). The mean wind speeds along the downwind ridge measured by the lidars are 1.8 m s^{-1} higher during northeasterly flow and 0.3 m s^{-1} for southwesterly flows. ~~This increase in wind speed can most likely be explained by the speed up that is caused by the formation of atmospheric waves during stable conditions (Palma et al., 2019)~~. Moreover, the mast measurements show consistently negative wind shear during stable conditions at both masts and as expected, lower levels of turbulence intensity and energy dissipation turbulent kinetic energy (Table 3).

15 During unstable atmospheric conditions, wind speeds are higher at the SW ridge for both flow directions. Remarkable is also the large flow inclination angles measured by the sonics at the upstream ridges of 12.12° (7.09°) for SW flow (NE flow). The much higher flow inclination angle for SW flow over the SW ridge supports the findings of Menke et al. (2018b) that the wind turbine wake is lifted higher during the day (unstable) than during the night (stable).

5.3 Comparison of lidar measurements and simulations

20 As described in section 3, we compare the ridge scan measurements to the WRF-LES simulations with and without forest drag implementation. Data from both simulations are extracted at the coordinates of the ridge scan points and interpolated to the exact measurement periods in time.

The best agreement, considering all available ridge scan periods, is reached for the WRF_NF simulation without forest 25 drag in terms of mean difference, root mean square error and bias. In this case, the WRF model is overestimating the wind speeds by 6.5% and 4.1% at the SW ridge and NE ridge, respectively (see Table 4). The WRF_F simulation with forest drag implementation underestimates the wind speeds along the ridges by -35.2% (-32.2%) at the SW (NE) ridge. This underestimation of simulated wind speeds on the ridge tops was also observed by Wagner et al. (2019b) and is most likely caused by an over-representation of the forest drag due to incorrect forest coverage on the ridge tops and too high trees in the 30 model. As described in section 3 an average canopy height of 30 m was used, whereas real tree heights obtained from an aerial laser scan in 2015 were in the order of 15 m (see Fig. 1b). The distribution of forested areas in Fig. 1b further indicates that the ridge tops were mostly free of trees, whereas both ridge tops are forested in the model according to the CORINE landuse data set (see Fig. 3 in Wagner et al., 2019b).

Table 3. Observation from tower tse04 (SW ridge) and tse13 (NE ridge). Turbulence intensity is defined as $TI = \sigma_U \overline{U}_{\text{sonic}}^{-1}$ where $\overline{U}_{\text{sonic}}$ is the mean wind speed and σ_U the standard deviation of U_{sonic} . Turbulent kinetic energy is calculated as $e = \frac{1}{2} [\overline{u'^2} + \overline{v'^2} + \overline{w'^2}]$, where u' , v' and w' are the fluctuating parts of the wind vector components as measured by the sonic anemometers. Wind shear and veer are calculated over 60 m (40 m – 100 m AGL). The flow inclination angle τ is calculated as $\arctan(w\sqrt{u^2 + v^2})$, where u and v are the mean horizontal wind vector components, and w the vertical. All averages are taken over 10 minutes. $\overline{U}_{\text{lidar}}$ is the mean of the wind speeds measured by the lidars averaged over the entire ridge. $\overline{\sigma}_{\text{lidar}}$ is the standard deviations also averaged along the ridge. N is the number of available 10-minute periods.

		$\overline{U}_{\text{lidar}}$	$\overline{\sigma}_{\text{lidar}}/\overline{U}_{\text{lidar}}$	$\overline{U}_{\text{sonic}}$	TI	e	shear	veer	τ	N
southwesterly flow		(m s ⁻¹)	(%)	(m s ⁻¹)	(%)	(m ² s ⁻²)	(m s ⁻¹)	(° m ⁻¹)	(° m ⁻¹)	
stable	SW ridge	5.43	3.9	5.13	11.27	0.29	0.012	-0.074	4.18	14
	NE ridge	5.75	7.6	5.41	17.33	0.63	0.011	-1.036	1.75	
unstable	SW ridge	5.01	10.5	5.11	32.96	1.29	-0.006	0.029	12.12	21
	NE ridge	4.56	13.3	4.35	43.58	1.51	0.001	-0.003	5.57	
northeasterly flow										
stable	SW ridge	7.66	4.9	7.33	11.96	0.52	0.016	-0.073	-1.74	77
	NE ridge	5.90	5.3	6.09	8.52	0.18	0.020	-0.147	0.67	
unstable	SW ridge	5.67	10.0	5.70	30.94	1.37	-0.001	0.084	2.90	39
	NE ridge	5.10	8.5	5.60	29.15	1.24	-0.001	-0.040	7.09	

Even though the simulation with forest drag underestimates wind speeds at the ridges, it shows improved correlation with the measurements (see Table 4). Correlation coefficients are consistently better for southwesterly wind directions and better or similar to the correlations of the simulation without forest drag for northeasterly flow. A comparison of the same simulations with multiple meteorological masts across the double ridge along transect southeast (TSE; equal to transect 2 in Fernando et al., 2019) in Wagner et al. (2019b) shows a clear improvement of simulated wind speeds in the WRF_F simulation with forest parameterization. This means that the forest parameterization enhances the simulated flow especially along the slopes of the ridges, where wind speeds are overestimated in the WRF_NF simulation. When comparing the simulations only to the two 100 m towers tse04 (T20) and tse13 (T29) on the SW and NE ridge, respectively, the WRF_F run underestimates wind speeds at 80 m AGL, but shows improved correlation values and root-mean-square errors (RMSE) (see Table 5 in this paper and Table 4 in Wagner et al., 2019b). The better results for the WRF_F run for the comparison with tse04 and tse13 may be induced by the larger number of samples that are available in the tower data set (about 13500 data points) compared to lidar data (507 points in time) representing a larger spectrum of different meteorological conditions.

Segregating the data into different atmospheric conditions shows that the WRF_NF run performs best under stable atmospheric conditions (Table 4). For unstable conditions, the WRF_F simulation performs better at the NE ridge and for northeasterly wind also at the SW ridge. Considering that the flow is more turbulent under unstable conditions, it can be assumed that

Table 4. Mean difference of WRF simulations and ridge scans calculated as $(U_{\text{WRF}} - U_{\text{lidar}}) U_{\text{lidar}}^{-1} \cdot 100$ and averaged along the entire ridge. Correlation coefficient (COR) and root mean square error (RMSE) values for the comparison of WRF data with the ridge scan measurements. The first number states the value for the WRF_NF simulation without forest and in brackets the value for the WRF_F run with forest parameterization. Bold values indicating the best model per parameter. The percentage of lidar observations, which describe the respective flow condition is indicated in the last column.

all directions		Mean difference (%)	COR	RMSE (m s^{-1})	bias (m s^{-1})	Fraction of used data (%)
all	SW ridge	6.5 (-35.2)	0.43 (0.49)	2.76 (3.43)	-0.07 (-2.52)	100
	NE ridge	4.1 (-32.2)	0.46 (0.44)	2.78 (2.94)	-0.16 (-2.09)	
stable	SW ridge	-3.6 (-39.0)	0.40 (0.52)	2.68 (3.68)	-0.77 (-2.91)	57.4
	NE ridge	-9.9 (-36.1)	0.48 (0.48)	2.56 (2.90)	-0.83 (-2.27)	
unstable	SW ridge	25.1 (-29.1)	0.50 (0.47)	2.83 (2.90)	1.19 (-1.89)	37.1
	NE ridge	29.9 (- 24.2)	0.44 (0.42)	3.06 (2.86)	1.11 (-1.69)	
southwesterly flow						
all	SW ridge	9.0 (-36.6)	0.38 (0.45)	2.61 (2.65)	-0.01 (-1.96)	9.3
	NE ridge	10.3 (-43.5)	0.40 (0.43)	3.49 (3.06)	0.06 (-2.41)	
stable	SW ridge	0.0 (-42.4)	0.19 (0.46)	2.19 (2.99)	-0.51 (-2.41)	2.8
	NE ridge	-22.1 (-56.4)	0.35 (0.40)	3.24 (4.08)	-1.75 (-3.55)	
unstable	SW ridge	30.4 (-32.7)	0.43 (0.54)	2.84 (2.17)	1.08 (-1.50)	4.1
	NE ridge	53.8 (- 39.7)	0.46 (0.49)	4.05 (2.54)	2.39 (- 1.85)	
northeasterly flow						
all	SW ridge	-6.6 (-30.8)	0.40 (0.41)	2.97 (3.87)	-0.96 (-2.63)	22.9
	NE ridge	-1.3 (-23.7)	0.43 (0.43)	2.82 (2.68)	-0.44 (-1.61)	
stable	SW ridge	-20.1 (-43.2)	0.43 (0.45)	3.20 (4.44)	-1.90 (-3.63)	15.2
	NE ridge	-19.1 (-35.3)	0.45 (0.45)	2.91 (3.09)	-1.39 (-2.28)	
unstable	SW ridge	19.9 (- 6.2)	0.51 (0.48)	2.35 (2.22)	0.93 (- 0.62)	7.7
	NE ridge	33.7 (- 0.7)	0.48 (0.49)	2.68 (1.73)	1.44 (- 0.25)	

Table 5. As in Table 4, but for comparison of WRF simulations with tower T20 (tse04) and T29 (tse13) on the SW and NE ridge, respectively.

all directions		Mean difference (%)	COR	RMSE (m s^{-1})	bias (m s^{-1})
all	T20	31.0 (- 23.1)	0.44 (0.65)	3.18 (2.35)	1.49 (- 1.11)
	T29	23.1 (-29.2)	0.46 (0.56)	3.03 (2.45)	1.07 (-1.35)

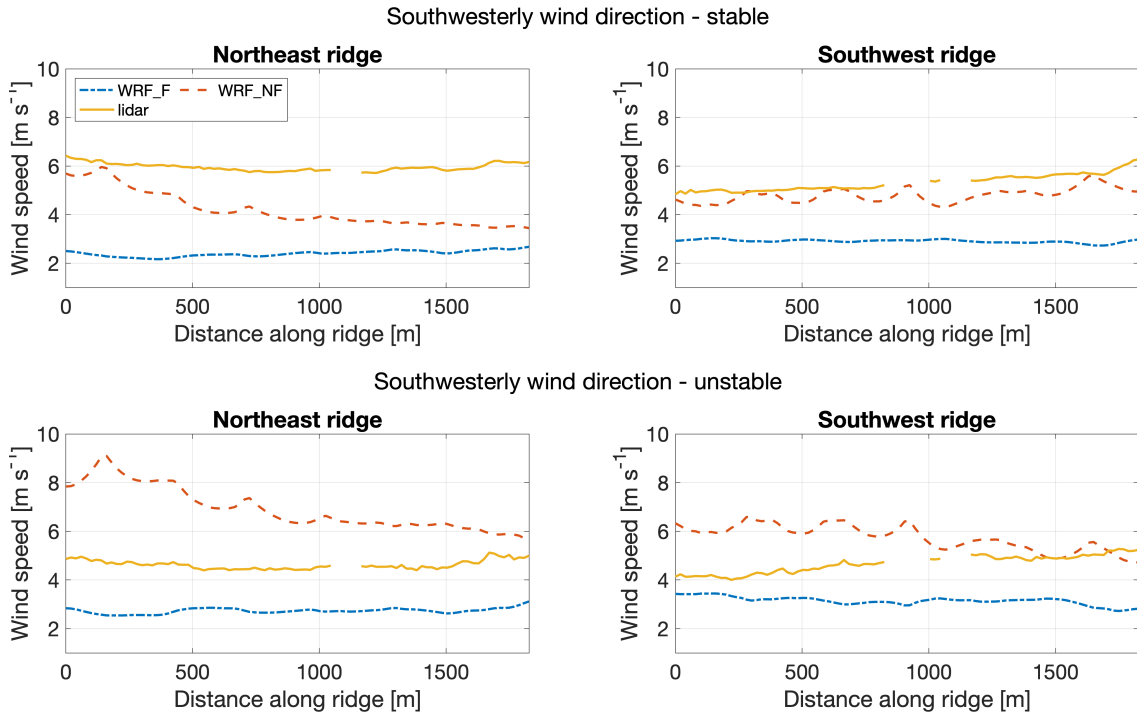


Figure 6. Comparison of WRF wind speeds and lidar ridge scan measurements for southwesterly flow segregated into stable and unstable conditions.

more mixing and interaction with the forest is taking place compared to stable conditions during which the forest rather acts as a displacement. For northeasterly winds, the high forest density for the fetch upstream of the NE ridge (see Figure 3 in Wagner et al., 2019b) might lead to better results of WRF with forest drag.

Figure 6 shows the spatial distribution of averaged wind speeds along the SW and NE ridges during southwesterly flow. The general underestimation of wind speeds in the WRF_F simulation is visible. Disregarding this negative offset, the WRF_F simulation shows spatial changes of wind speed along the ridges that are more similar to changes measured with the lidars compared to stronger gradients along the ridges in the WRF_NF simulation.

6 Discussion

The results and observations outlined above demonstrate the ability of the SLs to perform flow measurements over large areas. The design of the scanning scenario allowed us to capture fine differences in the flow field along the two ridges at Perdigão. Here we want to discuss three of the observed flow characteristics. Firstly, we observed on average a slow down of the flow at the terrain dip which seems to be in accordance with the classical linear flow perturbation theory. Apparently, the influence of channeling effects, which are expected under stably stratified conditions as described by Vassallo et al. (2020), is not significant

enough to affect the mean wind. Most likely the ratio of ridge height to dip height is too large to cause channeling effects that have a significant influence on the mean flow field at 80 m height AGL i.e. heights of interest for wind energy production.

Secondly, we want to focus the discussion at the observed wind speed changes along the SW ridge. The linear theory says that orography gives the same speed up if the sign of the wind vector changes. Accordingly, if orography is solely responsible for the speed up along the ridge the trend would be the same whether the wind is from the SW or NE. As we observed the direct opposite, for SW wind directions flow speed are highest in the SE end of the SW ridge and higher flow speeds in the NW end for NE wind directions, we can conclude that orography is not solely responsible. Likely is that the trend observed along the SW ridge is an interaction of orography and roughness effects. For roughness contrary to orography the speed up along the ridge is only affected by the roughness (i.e. the friction drag) of the terrain upstream. This explains the lower wind speeds in the SE of the SW ridge for NE winds as the density of larger trees increases to the SE (Figure 1b). For SW winds the higher winds in the SE end are most likely caused by an increasing steepness of the terrain and a decreasing steepness of the terrain from the NW towards the SE (Figure 1a and Menke et al. (2018b, Figure 2)).

Lastly, we want to focus on the flow observations under stably stratified conditions. The higher wind speeds observed at the downstream ridges under these conditions as described in (Section 5.2.2) are explainable by the speed up that is caused by the formation of atmospheric waves during stable conditions as shown in Palma et al. (2019) and Fernando et al. (2019, Figure 7d).

The observations show that as expected the flow is as complex as the terrain. Thus, reproducing the flow conditions with simulations is challenging as shown by the comparison with WRF-LES simulation results (Section 5.3). Summarizing, we find a high sensitivity of the WRF-LES simulations to the parameterization of surface friction. Adding a forest drag term significantly changes the results. The comparison of the simulations with the lidar ridge scans reveals that the forest drag is too strong on the ridge tops, which results in underestimated wind speeds. Without forest drag, wind speeds are overestimated on average. The comparison of the same simulations with multiple meteorological towers across the double ridge in Wagner et al. (2019b) shows an improvement of the simulated flow with forest parameterization. Also, relative changes in wind speed along the ridges are more similar for the simulation with forest drag when comparing to the relative changes observed with the WindScannersSLs. This shows that the forest parameterization has a positive effect on simulated wind speeds over Perdigão, but makes clear that the horizontal distribution of forested areas and the tree heights have to be more realistic in future model setups. This will only be possible by using the high-resolution aerial lidar high-resolution aerial laser scans used for the canopy height estimation in figure 1b, or by introducing better landuse land-use data sets, which include seasonal variability of the canopy layer, e.g., caused by forestry and agriculture.

30 7 Conclusions

The present lidar measurements demonstrate the ability of scanning lidars to perform wind resource measurements over large areas in complex terrain. Horizontal mean velocity profiles of 1.8 km length along ridges were retrieved and flow patterns during specific atmospheric conditions could be identified. The data were collected during the intensive measurement period

in May and June 2017 of the Flow over complex terrain causes challenges for wind energy projects. High spatial variability makes the selection of sites for wind turbines far from obvious. Capturing the spatial variability with measurements and flow simulation is generally challenging. On the measurement site, the spatial variability can be addressed by increasing the number of measurement locations. This can be done with scanning lidars as they can provide wind measurements over areas of several square kilometer. For simulating the flow advanced highly-resolved computer models are needed.

In our study, we present measurements of two pairs of SLs that were designed to assess the flow conditions at locations favorable for wind turbines during the Perdigão measurement campaign. An optimized filter for the lidar data is presented which yields in average to 20% more data compared to traditional filtering methods. Correlations of lidar and mast data show good agreement with correlation coefficients of 0.994 or better for line-of-sight velocities and 0.94 or better for horizontal wind speeds. We found that the lidar elevation angles have a negligible effect on the retrieved horizontal winds.

Considering all lidar measurements we find 10% higher wind speeds at the SW ridge. Segregating the data by wind direction reveals a gradient in wind speeds along the SW ridge, with increasing wind speeds from the NW to SE during southwesterly flows. The effect is reversed for northeasterly flows and amounts for both directions to a change of 14% in relative wind speed along the ridge. During stable atmospheric conditions, wind speeds are found to be highest at the downstream ridge independent of the wind direction. The mean wind speeds along the downwind ridge measured by the lidars are The SLs retrieve the horizontal mean velocity profiles of 1.8 m s^{-1} and 0.3 m s^{-1} higher during northeasterly and southwesterly flows, respectively km length along two ridges. We find a good correlation of the lidar measurements with sonic wind measurements at masts along on ridges. Moreover, we show that using advanced lidar data filtering methods improves the measurement availability by 20%. Our analysis of the flow fields along the ridges demonstrates the ability of the SLs to reveal significant details about the flow that would remain unrecognized when only few measurement locations are available.

The lidar observations have been compared to comparison of measurements and two WRF-LES simulations with and without forest drag implementation. The results show the best agreement, considering all available periods, for the WRF-LES run without forest drag. In that case, the simulation is overestimating the mean wind speeds along the SW ridge by 6.5% and by 4.1% along the NE ridge. Under unstable atmospheric conditions and northeasterly flow direction, the simulation with forest performs best. The simulation with forest drag has a better correlation coefficient but consistently underestimates the wind speeds at the ridges by 30–40% reveals a high sensitivity of the model to the parameterization of surface friction causing significant deviations between measurements and simulation. It is assumed that a wrong forest distribution in the model on the ridge tops and a overrated tree height are the main reason for the poor agreement of the simulation with additional forest parameterization. However, this study and Wagner et al. (2019b) show a considerably improved correlation of measurements and simulation when the parameterization is used.

Overall, we conclude that scanning lidar SL measurements are a valuable tool to asses assess wind resources in complex terrain. They help to understand the flow conditions and to validate simulations which are still challenged by the complexity of the topography. In the future, the system availability has to be improved SL system availability, which was only at 44% for the period investigated in this study. Main has to be improved. The main factors influencing the availability were software issues, hardware failures, and power outages. The comparison of measurements and flow simulations revealed a high sensitivity of

the model to the parameterization of surface friction. In contrast to this study, Wagner et al. (2019b) could show that the forest parameterization considerably improves the boundary layer flow over Perdigão when comparing simulations to meteorological towers across the double ridge. It is assumed that the wrong forest distribution in the model on the ridge tops and the overrated tree heights are the main reason for the poor agreement of WRF_F wind speeds with lidar ridge scans. This shows that aerial lidar scans as used by Boudreault et al. (2015) or more realistic landuse data sets, Moreover, we recommend to base flow simulations on as realistic as possible land-use data as e.g. acquired by Boudreault et al. (2015) and to including seasonal variability of the canopy distribution, are required as input for flow calculations in the future.

5

Data availability. The scanning lidar data for the entire measurement campaign is made available by Menke et al. (2018a). The measurement mast data is made available by NCAR for the 5 minute averaged data (UCAR/NCAR - Earth Observing Laboratory, 2019b) and for high-resolution data (UCAR/NCAR - Earth Observing Laboratory, 2019a).

Author contributions. Conceptualization, R.M., J.M. and N.V.; Methodology, R.M., J.M., N.V., S.O. and J.W.; Software, R.M. and J.W.;
5 Validation, R.M., J.M., N.V. and J.W.; Formal Analysis, R.M.; Investigation, R.M., J.M., N.V., S.O. and J.W.; Resources, R.M., J.M., N.V.,
S.O. and J.W.; Data Curation, R.M., S.O. and J.W.; Writing - Original Draft, R.M., J.M., N.V., S.O. and J.W.; Writing - Review & Editing,
R.M., J.M., N.V., S.O. and J.W.; Visualization, R.M.; Project Administration, J.M. and N.V.; Funding Acquisition, J.M. and S.O.

Competing interests. The authors declare that they have no conflict of interest.

Acknowledgements. We acknowledge the work of everyone involved in the planning and execution of the campaign, in specific we would
10 like to thank Stephan Voß, Julian Hieronimus (ForWind, University of Oldenburg), Per Hansen and Preben Aagaard (DTU Wind Energy) for
their help with the installation of the [WindScanners](#)scanning lidars. We are also grateful for the contribution of three [WindScanners](#)scanning
lidars to the campaign by ForWind. Moreover, only the intensive negotiations of José Carlos Matos, INEGI with local landowners about
specific locations for our [WindScanners](#)scanning lidars made this research possible. We are grateful to the municipality of Vila Velha de
Ródão, landowners who authorized installation of scientific equipment in their properties, the residents of Vale do Cobrão, Foz do Cobrão,
15 Alvaiade, Chão das Servas and local businesses who kindly contributed to the success of the campaign. The space for operational centre was
generously provided by Centro Sócio- Cultural e Recreativo de Alvaiade in Vila Velha de Rodão. We thank the Danish Energy Agency for
funding through the New European Wind Atlas project (EUDP 14-II). The contribution of R. Menke are partly based upon work supported
by the National Center for Atmospheric Research, which is a major facility sponsored by the National Science Foundation under Cooperative
Agreement No. 1852977. Any opinions, findings and conclusions or recommendations expressed in this material do not necessarily reflect
20 the views of the National Science Foundation.

References

- Bechmann, A., Sørensen, N. N., Berg, J., Mann, J., and Réthoré, P.-E.: The Bolund Experiment, Part II: Blind Comparison of Microscale Flow Models, *Boundary-Layer Meteorology*, 141, <https://doi.org/10.1007/s10546-011-9637-x>, 2011.
- Beck, H. and Kühn, M.: Dynamic Data Filtering of Long-Range Doppler LiDAR Wind Speed Measurements, *Remote Sensing*, 9, 5, <https://doi.org/10.3390/rs9060561>, 2017.
- Berg, J., Troldborg, N., Menke, R., Patton, E. G., Sullivan, P. P., Mann, J., and Sørensen, N.: Flow in complex terrain - a Large Eddy Simulation comparison study, *Journal of Physics: Conference Series*, 1037, 072015, <https://doi.org/10.1088/1742-6596/1037/7/072015>, 2018.
- Bingöl, F., Mann, J., and Foussekis, D.: Conically scanning lidar error in complex terrain, *Meteorologische Zeitschrift*, 18, 189–195, 10, <https://doi.org/10.1127/0941-2948/2009/0368>, 2009.
- Bingöl, F., Mann, J., and Larsen, G. C.: Light detection and ranging measurements of wake dynamics part I: one-dimensional scanning, *Wind Energy: An International Journal for Progress and Applications in Wind Power Conversion Technology*, 13, 51–61, <https://doi.org/10.1002/we.352>, 2010.
- Bodini, N., Zardi, D., and Lundquist, J. K.: Three-dimensional structure of wind turbine wakes as measured by scanning lidar, *Atmospheric Measurement Techniques*, 10, 2881–2896, <https://doi.org/10.5194/amt-10-2881-2017>, 2017.
- Boudreault, L.-É., Bechmann, A., Tarvainen, L., Klemedtsson, L., Shendryk, I., and Dellwik, E.: A LiDAR method of canopy structure retrieval for wind modeling of heterogeneous forests, *Agricultural and Forest Meteorology*, 201, 86–97, <https://doi.org/10.1016/j.agrformet.2014.10.014>, 2015.
- Clifton, A., Clive, P., Gottschall, J., Schlipf, D., Simley, E., Simmons, L., Stein, D., Trabucchi, D., Vasiljevic, N., and Würth, 20: I.: IEA Wind Task 32: Wind lidar identifying and mitigating barriers to the adoption of wind lidar, *Remote Sensing*, 10, 406, <https://doi.org/10.3390/rs10030406>, 2018.
- Fernando, H., Mann, J., Palma, J., Lundquist, J., Barthelmie, R., BeloPereira, M., Brown, W., Chow, F., Gerz, T., Hocut, C., Klein, P., Leo, L., Matos, J., Oncley, S., Pryor, S., Bariteau, L., Bell, T., Bodini, N., Carney, M., Courtney, M., Creegan, E., Dimitrova, R., Gomes, S., Hagen, M., Hyde, J., Kigle, S., Krishnamurthy, R., Lopes, J., Mazzaro, L., Neher, J., Menke, R., Murphy, P., Oswald, L., Otarola-Bustos, 25 S., Pattantyus, A., Rodrigues, C. V., Schady, A., Sirin, N., Spuler, S., Svensson, E., Tomaszewski, J., Turner, D., van Veen, L., Vasiljević, N., Vassallo, D., Voss, S., Wildmann, N., and Wang, Y.: The Perdigão: Peering into Microscale Details of Mountain Winds, *Bulletin of the American Meteorological Society*, <https://doi.org/10.1175/BAMS-D-17-0227.1>, 2019.
- Iungo, G. V., Wu, Y.-T., and Porté-Agel, F.: Field Measurements of Wind Turbine Wakes with Lidars, *Journal of Atmospheric and Oceanic Technology*, 30, 274–287, <https://doi.org/10.1175/JTECH-D-12-00051.1>, 2013.
- Käsler, Y., Rahm, S., Simmet, R., and Kühn, M.: Wake Measurements of a Multi-MW Wind Turbine with Coherent Long-Range Pulsed Doppler Wind Lidar, *Journal of Atmospheric and Oceanic Technology*, 27, 1529–1532, <https://doi.org/10.1175/2010JTECHA1483.1>, 2010.
- Lange, J., Mann, J., Angelou, N., Berg, J., Sjöholm, M., and Mikkelsen, T.: Variations of the Wake Height over the Bolund Escarpment Measured by a Scanning Lidar, *Boundary-Layer Meteorology*, 159, 147–159, <https://doi.org/10.1007/s10546-015-0107-8>, 2016.
- 35 Lange, J., Mann, J., Berg, J., Parvu, D., Kilpatrick, R., Costache, A., Chowdhury, J., Siddiqui, K., and Hangan, H.: For wind turbines in complex terrain, the devil is in the detail, *Environmental Research Letters*, 12, 094020, <https://doi.org/10.1088/1748-9326/aa81db>, 2017.

- Lehner, M., Rotunno, R., and Whiteman, C. D.: Flow Regimes over a Basin Induced by Upstream Katabatic Flows - An Idealized Modeling Study, *Journal of the Atmospheric Sciences*, 73, 3821–3842, <https://doi.org/10.1175/JAS-D-16-0114.1>, 2016.
- Mann, J., Angelou, N., Arnqvist, J., Callies, D., Cantero, E., Arroyo, R. C., Courtney, M., Cuxart, J., Dellwik, E., Gottschall, J., Ivanell, S., Kühn, P., Lea, G., Matos, J. C., Palma, J. M. L. M., Pauscher, L., Peña, A., Rodrigo, J. S., Söderberg, S., Vasiljevic, N., and Rodrigues, C. V.: Complex terrain experiments in the New European Wind Atlas, *Philosophical Transactions of the Royal Society A: Mathematical, Physical and Engineering Sciences*, 375, 20160 101, <https://doi.org/10.1098/rsta.2016.0101>, 2017.
- Mann, J., Diaz, A. P., Troldborg, N., and Andersen, S. J.: How does turbulence change approaching a rotor?, *Wind Energy Science*, 3, 293–300, <https://doi.org/10.5194/wes-3-293-2018>, 2018.
- Menke, R., Mann, J., and Vasiljevic, N.: Perdigão-2017: multi-lidar flow mapping over the complex terrain site, <https://doi.org/10.11583/DTU.7228544.v1>, 2018a.
- Menke, R., Vasiljevic, N., Hansen, K., Hahmann, A. N., and Mann, J.: Does the wind turbine wake follow the topography? - A multi-lidar study in complex terrain, *Wind Energy Science*, p. 18, <https://doi.org/10.5194/wes-3-681-2018>, 2018b.
- Menke, R., Mann, J., and Svensson, E.: Perdigão 2017: GPS survey of sonic anemometers and WindScanners operated by DTU, DTU Wind Energy, Denmark, 2019a.
- Menke, R., Vasiljević, N., Mann, J., and Lundquist, J. K.: Characterization of flow recirculation zones at the Perdigão site using multi-lidar measurements, *Atmospheric Chemistry and Physics*, 19, 2713–2723, <https://doi.org/10.5194/acp-19-2713-2019>, 2019b.
- Mikkelsen, T., Angelou, N., Hansen, K., Sjöholm, M., Harris, M., Slinger, C., Hadley, P., Scullion, R., Ellis, G., and Vives, G.: A spinner-integrated wind lidar for enhanced wind turbine control, *Wind Energy*, 16, 625–643, <https://doi.org/10.1002/we.1564>, 2013.
- Palma, J., Lopes, A. S., Gomes, V. C., Rodrigues, C. V., Menke, R., Vasiljević, N., and Mann, J.: Unravelling the wind flow over highly complex regions through computational modeling and two-dimensional lidar scanning, *Journal of Physics: Conference Series*, 1222, 012006, <https://doi.org/10.1088/1742-6596/1222/1/012006>, 2019.
- Pauscher, L., Vasiljevic, N., Callies, D., Lea, G., Mann, J., Klaas, T., Hieronimus, J., Gottschall, J., Schwesig, A., Kühn, M., and Courtney, M.: An Inter-Comparison Study of Multi- and DBS Lidar Measurements in Complex Terrain, *Remote Sensing*, 8, <https://doi.org/10.3390/rs8090782>, 2016.
- Pineda, N., Jorba, O., Jorge, J., and Baldasano, J. M.: Using NOAA AVHRR and SPOT VGT data to estimate surface parameters: application to a mesoscale meteorological model, *International Journal of Remote Sensing*, 25, 129–143, <https://doi.org/10.1080/0143116031000115201>, 2004.
- Sathe, A. and Mann, J.: A review of turbulence measurements using ground-based wind lidars, *Atmospheric Measurement Techniques*, 6, 3147–3167, <https://doi.org/10.5194/amt-6-3147-2013>, 2013.
- Shaw, T. H. and Schumann, U.: Large-eddy simulation of turbulent flow above and within a forest, *Bound.-Layer Meteor.*, 61, 47–64, <https://doi.org/10.1007/BF02033994>, 1992.
- Simley, E., Angelou, N., Mikkelsen, T., Sjöholm, M., Mann, J., and Pao, L. Y.: Characterization of wind velocities in the upstream induction zone of a wind turbine using scanning continuous-wave lidars, *Journal of Renewable and Sustainable Energy*, 8, 013301, <https://doi.org/10.1063/1.4940025>, 2016.
- Skamarock, W. C., Klemp, J. B., Dudhia, J., Gill, D. O., Barker, D. M., Duda, M. G., Huang, X.-Y., Wang, W., and Powers, J. G.: A description of the Advanced Research WRF Version 3, NCAR technical note, Mesoscale and Microscale Meteorology Division, National Center for Atmospheric Research, Boulder, Colorado, USA, http://www2.mmm.ucar.edu/wrf/users/docs/arw_v3.pdf, 2008.

- Trujillo, J.-J., Bingöl, F., Larsen, G. C., Mann, J., and Kühn, M.: Light detection and ranging measurements of wake dynamics. Part II: two-dimensional scanning, *Wind Energy*, 14, 61–75, <https://doi.org/10.1002/we.402>, 2011.
- UCAR/NCAR - Earth Observing Laboratory: NCAR/EOL Quality Controlled High-rate ISFS surface flux data, geographic coordinate, tilt corrected. Version 1.1, <https://doi.org/10.26023/8x1n-tct4-p50x>, 2019a.
- 5 UCAR/NCAR - Earth Observing Laboratory: NCAR/EOL Quality Controlled 5-minute ISFS surface flux data, geographic coordinate, tilt corrected. Version 1.1, <https://doi.org/10.26023/zdmj-d1ty-fg14>, 2019b.
- Vasiljevic, N.: A time-space synchronization of coherent Doppler scanning lidars for 3D measurements of wind fields, Ph.D. thesis, Denmark, 2014.
- Vasiljevic, N., Lea, G., Courtney, M., Cariou, J.-P., Mann, J., and Mikkelsen, T.: Long-range WindScanner system, *Remote Sensing*, p. 26, 10 <https://doi.org/10.3390/rs8110896>, 2016.
- Vasiljević, N., Vignaroli, A., Bechmann, A., and Wagner, R.: Digitizing scanning lidar measurement campaign planning, *Wind Energy Science Discussions*, 2019, 1–28, <https://doi.org/10.5194/wes-2019-13>, 2019.
- Vasiljević, N., Palma, J. M. L. M., Angelou, N., Matos, J. C., Menke, R., Lea, G., Mann, J., Courtney, M., Ribeiro, L. F., and Gomes, V. M. M. G. C.: Perdigão 2015: methodology for atmospheric multi-Doppler lidar experiments, *Atmospheric Measurement Techniques*, pp. 15 1–28, <https://doi.org/10.5194/amt-2017-18>, 2017.
- Vassallo, D., Krishnamurthy, R., Menke, R., and Fernando, H. J.: Observations of stably stratified flow through a microscale gap, *Journal of Atmospheric Sciences*, submitted, 2020.
- Wagner, J., Gerz, T., Wildmann, N., and Gramitzky, K.: Long-term simulation of the boundary layer flow over the double-ridge site during the Perdigão 2017 field campaign, *Atmospheric Chemistry and Physics*, 19, 1129–1146, <https://doi.org/10.5194/acp-19-1129-2019>, 2019a.
- 20 Wagner, J., Wildmann, N., and Gerz, T.: Improving boundary layer flow simulations over complex terrain by applying a forest parameterization in WRF, *Wind Energy Science Discussions*, <https://doi.org/10.5194/wes-2019-77>, in review, 2019b.